Article:
Smallcombe, J., Garnsworthy, A. B., Korten, W. et al. (26 more authors) (2024) Reevaluation of structures in Se 70 from combined conversion-electron and y -ray spectroscopy. Physical Review C. 024318. ISSN 2469-9993

https://doi.org/10.1103/PhysRevC.110.024318

Reevaluation of structures in ^{70}Se from combined conversion-electron and γ-ray spectroscopy

J. Smallcombe,[1,2,*] A. B. Garnsworthy,[3] W. Korten,[4] P. Singh,[4] D. Muir,[5] L. Próchniak,[6] F. A. Ali,[7,8] C. Andreoiu,[9] S. Ansari,[4] G. C. Ball,[3] C. J. Barton,[5] S. S. Bhattacharjee,[3] M. Bowry,[3,†] A. D. Briscoe,[2] R. Caballero-Folch,[3] A. Chester,[3,‡] S. A. Gillespie,[3,‡] G. F. Grinyer,[10] G. Hackman,[3] J. Heery,[11] C. Jones,[3,11] B. Melon,[12] M. Moukaddam,[11,§] A. Nannini,[12] P. Ruotsalainen,[13] K. Starosta,[9] C. E. Svensson,[7] R. Wadsworth,[5] and J. Williams[3]

[1]*Advanced Science Research Center, Japan Atomic Energy Agency (JAEA), Tokai, Ibaraki 319-1195, Japan*
[2]*Oliver Lodge Laboratory, University of Liverpool, Liverpool L69 9ZE, United Kingdom*
[3]*TRIUMF, 4004 Wesbrook Mall, Vancouver, British Columbia V6T 2A3, Canada*
[4]*Irfu, CEA, Université Paris-Saclay, F-91191 Gif-sur-Yvette, France*
[5]*School of Physics, Engineering and Technology, University of York, Heslington, York YO10 5DD, United Kingdom*
[6]*Heavy Ion Laboratory, University of Warsaw, PL-02-093 Warsaw, Poland*
[7]*Department of Physics, University of Guelph, Guelph, Ontario N1G 2W1, Canada*
[8]*Department of Physics, University of Sulaimani, P.O. Box 334, Sulaimani, Kurdistan Region, Iraq*
[9]*Department of Chemistry, Simon Fraser University, Burnaby, British Colombia V5A 1S6, Canada*
[10]*Department of Physics, University of Regina, Regina, Saskatchewan S4S 0A2, Canada*
[11]*Department of Physics, University of Surrey, Guildford, Surrey GU2 7XH, United Kingdom*
[12]*INFN Sezione di Firenze, I-50019 Firenze, Italy*
[13]*University of Jyväskylä, Department of Physics, P.O. Box 35, FI-40014, University of Jyväskylä, Finland*

(Received 22 March 2024; accepted 3 July 2024; published 20 August 2024)

Background: In the selenium isotopes various shape phenomena are present, in particular, the emergence of a dominant oblate deformation in the most neutron-deficient isotopes has been observed. The scenario of shape coexisting oblate and prolate bands has been proposed across the isotopic chain, with the crossing point of such bands being located near ^{70}Se, where no coexistence has yet been identified.
Purpose: To determine the presence or absence of any low-lying 0^+ state in ^{70}Se, confirm the level structure, and interpret the nuclear deformation with theoretical models.
Methods: A combined internal-conversion-electron and γ-ray spectroscopy study was undertaken with the SPICE and TIGRESS spectrometers at the TRIUMF-ISAC-II facility. Nuclear models were provided by the generalized triaxial rotor model (GTRM) and the collective generalised Bohr Hamiltonian (GBH).
Results: Despite a comprehensive search, no evidence was found for the existence of a 0^+ state below 2 MeV in ^{70}Se. Significant discrepancies to the previously established positive-parity-level scheme were found. GBH calculations using UNEDF1 mass parameters were found to reproduce the revised low-lying level structure well.
Conclusion: ^{70}Se does not have a well-defined axial shape. The 2_2^+ state at 1601 keV resembles a quasi-γ excitation rather than a member of a shape coexisting band; the presence of such a band is all but ruled out.

DOI: 10.1103/PhysRevC.110.024318

I. INTRODUCTION

One of the key questions for nuclear physics is how do the interactions of individual nucleons sum together to produce the collective behavior observed in nuclei. Shell model theory tells us that the orbitals that appear at the Fermi surface of a nucleus dominate its behavior. Energetically favorable symmetry breaking of these orbitals can thus lead to nuclear deformation. The occupation of different configurations of orbitals, corresponding to different shapes, may be equally favorable, leading to multiple shape minima, commonly referred to as shape coexistence.

However, matching such theoretical interpretation of nuclei within the intrinsic frame to the experimentally observable states is particularly challenging. In even-even nuclei, the presence of a low-lying 0^+ state is often taken as a fingerprint of shape coexistence [1–6]. However, observables which are

*Contact author: smallcombe.james@jaea.go.jp
†Present address: School of Engineering, Computing and Physical Sciences, University of the West of Scotland, High Street, Paisley PA1 2BE, United Kingdom.
‡Present address: Facility for Rare Isotope Beams, Michigan State University, East Lansing, Michigan 48824, USA.
§Present address: Universitè de Strasbourg, IPHC, 23 rue du Loess, 67037 Strasbourg, France.

more fundamentally related to the shape of the nucleus, such as quadrupole moments (Q_2) and transition strengths [$B(E2)$], as well as monopole transition strengths [$\rho^2(E0)$], are needed to accurately quantify both the deformation of these observed states and, crucially, the degree of mixing between them.

In the neutron-deficient Ge, Se, and Kr isotopes, a picture of shape coexistence has been formed over many years of study. Initially long-lived low-lying 0^+ shape-isomer states were identified, and through progressive measurements the picture of oblate-prolate coexistence in the region was reinforced [7–13].

Of particular interest have been the selenium isotopes, in which the question has long been debated of a possible transition from prolate to oblate dominance in the ground state as neutrons are removed approaching the $N = Z$ line [14–17]. Experimental measurements initially led to calculations which suggested a crossing point of these coexisting shapes at ^{72}Se [12]. Recent Coulomb excitation (Coulex) measurements of quadrupole moments suggest the ground state of this nucleus has a dominant prolate deformation [18]; however, the higher spin yrast states do display oblate characteristics, suggesting strong mixing and near degeneracy of the two shapes. Conversely, experimental measurements of ^{68}Se indicate a clearly oblate ground state [17]. The shape and nature of ^{70}Se remains ambiguous; past measurements suggested an oblate shape but these were inconclusive [11,19]. More recent measurements would seem to support an oblate assignment [20,21].

While it remains of interest to answer at which point in these isotopes the quadrupole moments of the nuclei change sign, it is also important to understand if the label of shape coexistence remains an accurate interpretation of their structures, and if such a picture can explain macroscopic observables. Indeed, it has become clear that a simple model of coexisting symmetric rotor bands does not fit the region. Significant triaxiality has been identified in germanium nuclei, including coexistence of two distinct triaxial shapes identified in experimental studies of ^{72}Ge [22]. It has also been shown through Coulex measurements of shape invariants of ^{76}Se that the lowest-lying states show significant triaxiality [23]. This pattern is reinforced by theoretical calculations which show that ^{72}Se and ^{70}Se are significantly γ soft, with ^{70}Se leaning more towards a vibrational-like structure than a rotor [24–26]. The latest calculations suggest ^{70}Se is soft in both β and γ, having no "well-defined shape" [27].

Beyond quadrupole deformation, octupole correlations have recently been demonstrated in ^{73}Br [28]. In this region the Fermi surface of both neutrons and protons are close to the "octupole magic number" 34, where interactions between the $\Delta l{=}\Delta j{=}3$ orbitals $p_{3/2}$ and $g_{9/2}$ can induce octupole correlations. Recent experimental studies further determined the presence of such correlations to some degree in ^{72}Se [24,29].

Among the many conclusions presented in the region, the shape and structure of ^{70}Se remains in dispute. Is ^{70}Se the critical crossing point of an oblate-prolate shape coexistence system, or perhaps a softly oblate triaxial vibrator? Under the shape coexistence picture, a band structure built upon a low-lying 0^+ state is predicted but has yet to be clearly identified. The 2_2^+ state has been identified as a possible member of such a band [30,31]. To conclusively identify any possibly unobserved 0^+ band head and further elucidate the level structure of ^{70}Se, an internal-conversion-electron and γ-ray spectroscopy study was undertaken.

II. EXPERIMENT

States in ^{70}Se were populated in the fusion-evaporation reaction ^{40}Ca(^{36}Ar, α2p)^{70}Se. A beam of ^{36}Ar at an energy of 120 MeV was delivered to a target at the center of the TRIUMF-ISAC Gamma-Ray Escape Suppressed Spectrometer (TIGRESS) [32] by the TRIUMF-ISAC-II superconducting LINAC [33,34] at an average current of 0.8 pnA for a period of 7 days. Results from this experiment related to ^{72}Se have been published in Ref. [35], and a full description of the experimental setup and calibrations is provided there. A primary target of 0.5 mg/cm^2 natural calcium was used, backed by a 15.7-mg/cm^2 silver layer to catch recoils. Following beam-target reactions, the emitted internal conversion electrons (ICE) were detected by SPICE [36,37], a permanent-magnet electron spectrometer, and γ rays were detected by the TIGRESS HPGe array. A downstream annular silicon detector recorded charged evaporation particles. Data were recorded to disk for every event in which a SPICE trigger was detected or for events in which a TIGRESS $\gamma\gamma$ coincidence trigger was detected. Data from the latter trigger condition were downscaled by a factor of 4 or 8, manually selected dependent on the data rate. An analysis of the γ-ray data was undertaken, leading to proposed changes to the previously assigned positive-parity structures of ^{70}Se. An analysis of ICE singles and ICE-γ coincidence data was undertaken to identify the presence of any 0^+ state associated with the band of the 1601-keV 2_2^+ state. Such a 0^+ state, lying close to (or below) the energy of the 2_1^+ state at 945 keV, is expected to have a significant (or exclusive) electric monopole ($E0$) decay to the ground state, making it possible to identify by ICE emission even in the case of minimal feeding from higher-lying states, or of feeding γ rays that are obscured by other more intense transitions.

III. RESULTS

A. Gamma-ray data

An analysis was undertaken of $\gamma\gamma$ and $\gamma\gamma\gamma$ matrices, and for counterpart γ matrices obtained from events in prompt coincidence with the detection of an α particle in the downstream silicon detector. This requirement preferentially selects evaporation channels with products which include ^{70}Se and significantly suppresses background contaminants, which includes ^{72}Se, ^{72,73}Br, ^{70}Ge, ^{197}Au, and ^{107,109}Ag. A selection of the data is shown in Fig. 1. In addition to confirming much of the structure previously reported, several new transitions and levels were identified. Significant discrepancies in γ-ray energies were found between the measured γ-ray dataset and those previously reported in literature. As recoiling nuclei came to rest in the stopper foil with a stopping time of $\approx$1 ps, this puts an effective lower limit on the lifetime of observed states. States with a lifetime of the order of the recoil stopping time have a significant Doppler broadening feature.

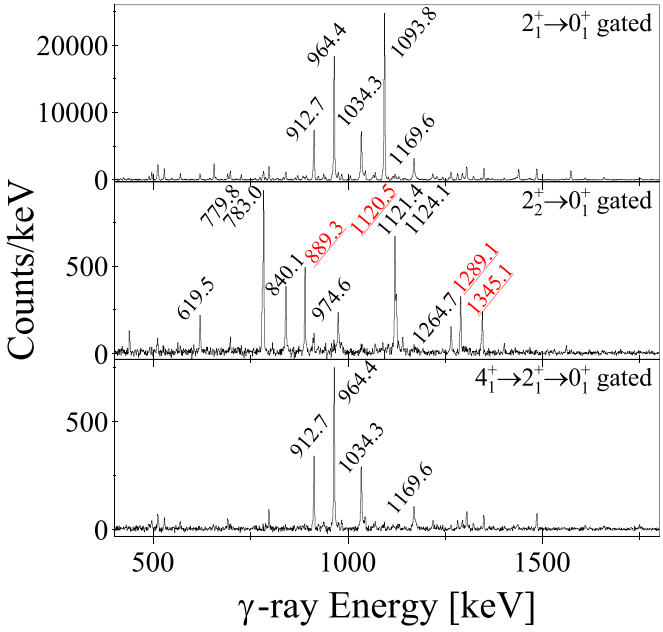

FIG. 1. Gamma-ray spectra from the projection of α-particle-coincident $\gamma\gamma$ and $\gamma\gamma\gamma$ matrices. Coincidence spectra are shown for the ^{70}Se 945-keV $2_1^+ \rightarrow 0_1^+$ transition (top), the 1601-keV $2_2^+ \rightarrow 0_1^+$ transition (middle), and for the double coincidence gate of 945-keV $2_1^+ \rightarrow 0_1^+$ and 1094-keV $4_1^+ \rightarrow 2_1^+$ γ rays (bottom). A continuum background subtraction has been applied to each of the spectra. Prominent peaks are labeled with the measured transition energy; these are underlined for transitions corresponding to contaminant ^{46}Ti.

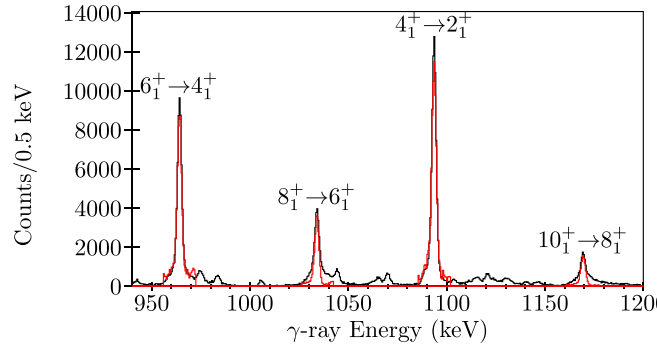

FIG. 2. Figure demonstrating the Doppler broadened peak shapes of short-lived yrast states in ^{70}Se. A spectrum gated on the $2_1^+ \rightarrow 0_1^+$ transition is shown (black). An second spectrum was produced by a sum of gates on 797-, 1305-, 1754-, and 1903-keV transitions, which feed the yrast band above the 10_1^+ state. Sections of this feeding spectrum are scaled and overlain (red). For the $10_1^+ \rightarrow 8_1^+$ and $8_1^+ \rightarrow 6_1^+$ γ rays, a decreased in-flight component can clearly be observed in the peak shapes of the spectrum gated on transitions from above.

The yrast band of ^{70}Se was populated up to the 14^+ state. For the higher-lying shorter-lived yrast states, it was possible to isolated the in-flight contribution of peaks. This was achieved by producing spectra gated on transitions feeding the yrast band above a given state, in which the peak shape is dominated by the stopped component, and comparing to spectra gated on transitions from lower-lying yrast states. One such gating comparison is shown in Fig. 2.

By fitting the stopped component of broadened peaks, using constrained peak-shape parameters, accurate energies and branching ratios were determined at the cost of absolute intensity determination. Gamma-ray fitting parameters were confirmed to reproduce the reported energies of known transitions of in-beam ^{72}Se and ^{107,109}Ag, and those of a ^{152}Eu calibration source. For transitions from the lowest-lying states in ^{70}Se, in which the stopped component is dominant, there is agreement between newly measured and previously reported γ-ray energies.

While the in-flight component largely forms a background beneath the stopped peaks, the configuration of TIGRESS was such that the mean γ-ray detection angle was $\approx 70^\circ$, leading to a positive mean Doppler shift. The exact shape of this background may cause an undue increase in fit centroid energies, despite the adopted fitting procedure. Such a systematic effect could not be experimentally confirmed or quantified without giving unjustified credence to previous datasets. As such, we report a complete set of measured γ-ray energies, intensities, and an independently derived level scheme. Discussions use the energies of this work.

The level scheme determined for ^{70}Se is shown in Fig. 3. Spin and parity assignments are given as certain for states which agree with existing datasets; the remaining tentative assignments are based predominately on an assumption of $E2$ dominated band structures. Energies and spin assignments of states, as well as energies and branching ratios of γ rays, are given in Table I.

1. Non-yrast positive-parity structure

The nature of the 1601-keV 2_2^+ state is particularly important to this study, as we aim to determine if this state is a member of a shape coexisting 0^+ band or perhaps a band head itself, i.e., for a $K = 2$ γ band. It is subsequently quite alarming to discover that the structure above the 1601-keV state is far more complex than previously thought. Above the 4_2^+ state at 2384 keV, significant discrepancy is found from the previous experimental results of Ref. [38]. The previously reported 6^+ state at 3218 keV is not observed, neither the depopulating 836- or 215-keV γ rays are identified, and none of the states above this are identified. A state which strongly feeds the 4_2^+ 2384-keV state, as well as the yrast 6_1^+ and 4_1^+ states, is identified at 3505 keV. This state also has a strong decay branch to a new state placed at 2725 keV, which circumvents the 4_2^+ state. The differences to Ref. [38], results from which are shown in Fig. 3 for comparison, can largely be attributed to the presence of several near degenerate transitions at around 1120 and 780 keV. These could not have been resolved with the resolution of the previous dataset, leading to confusion in the relative intensities and subsequent ordering of transitions. Whereas, with the aid of the thick target employed in this work, which removed any significant kinematic broadening from most of the observed transitions, a significantly improved resolution is achieved in the present data. Figure 4 demonstrates the doublet γ rays separated by careful gating. Further states are identified in this band at 4345 and 5320 keV, the placement of which are confirmed by identification of transitions linking

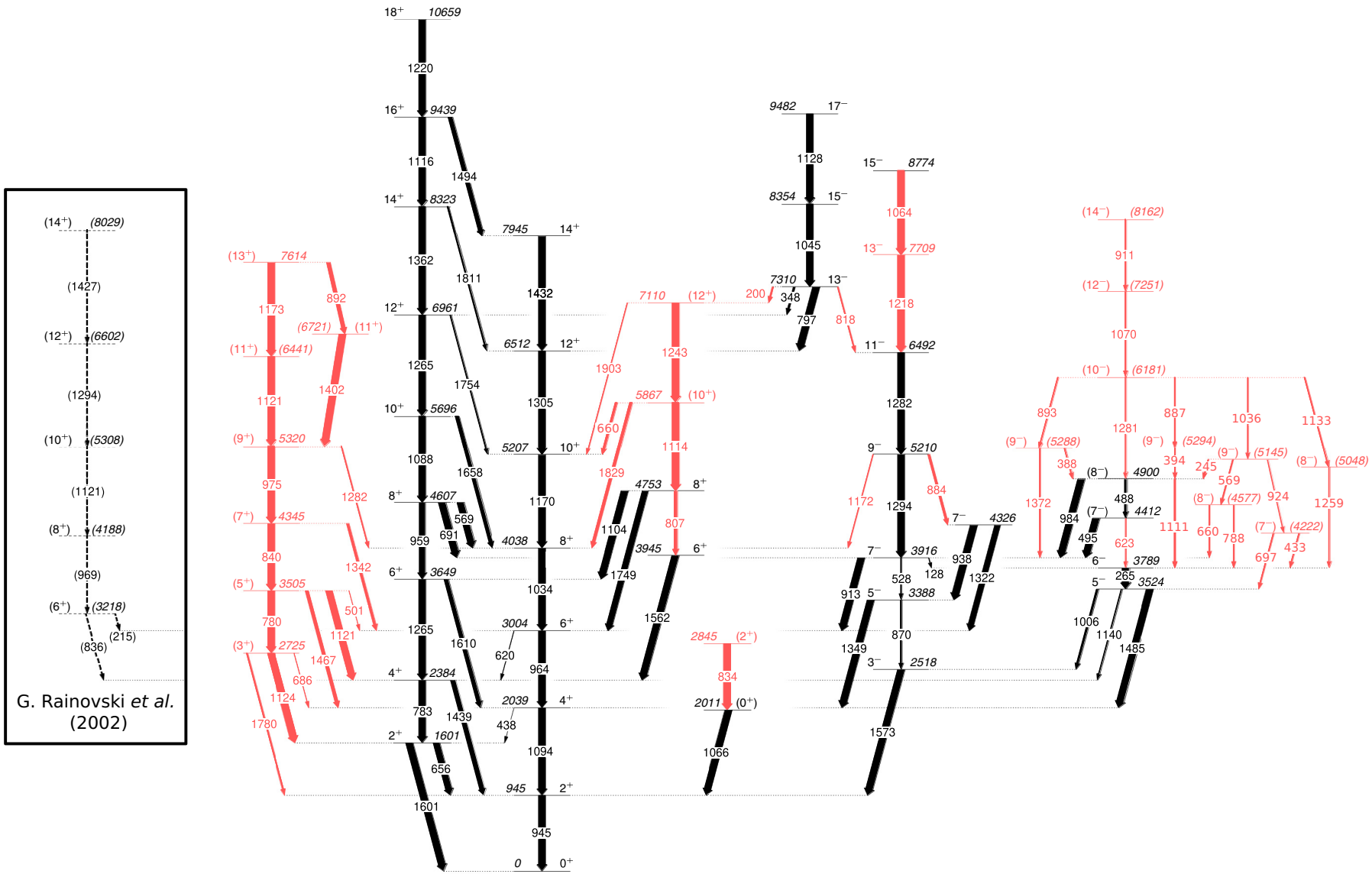

FIG. 3. ^{70}Se level scheme, as determined from the TIGRESS γ-ray data in this work. Arrow widths indicate the relative branching ratio for each level. New levels and γ rays are highlighted in red. See texts for discussion of assignments. An inset panel shows a partial level scheme from previous works [38,39] highlighting reported structure connected to the 4_2^+ state which are not observed in the present experiment.

TABLE I. Levels populated in ^{70}Se and their experimentally observed depopulating γ rays. The γ-ray branching ratios are normalized to the most intense transition for each state. State energies, γ-ray energies, and branching ratios are determined exclusively from the present dataset.

E_i (keV)	$(I_i^\pi) \rightarrow (I_f^\pi)$	E_γ (keV)	B_γ	E_f (keV)
945.29(1)	$2_1^+ \rightarrow 0_1^+$	945.29(1)	100	0
1601.0(1)	$2_2^+ \rightarrow 2_1^+$	655.7(1)	90(2)	945.29
	$2_2^+ \rightarrow 0_1^+$	1601.0(1)	100(2)	0
2011.1(2)	$(0_2^+) \rightarrow 2_1^+$	1065.8(2)	100	945.29
2039.08(3)	$4_1^+ \rightarrow 2_2^+$	437.8(3)	0.6(2)	1601.0
	$4_1^+ \rightarrow 2_1^+$	1093.79(3)	100.0(4)	945.29
2384.0(1)	$4_2^+ \rightarrow 2_2^+$	783.0(2)	100(6)	1601.0
	$4_2^+ \rightarrow 2_1^+$	1438.7(2)	70(5)	945.29
2518.2(1)	$3^- \rightarrow 2_1^+$	1573.0(2)	100	945.29
2725.3(1)	$(3_1^+) \rightarrow 4_1^+$	686.0(4)	5(2)	2039.08
	$(3_1^+) \rightarrow 2_2^+$	1124.1(4)	100(5)	1601.0
	$(3_1^+) \rightarrow 2_1^+$	1780.1(2)	20(3)	945.29
2844.8(4)	$(2_3^+) \rightarrow (0_2^+)$	833.7(3)	100	2011.1
3003.5(1)	$6_1^+ \rightarrow 4_2^+$	619.5(1)	4.4(3)	2384.0
	$6_1^+ \rightarrow 4_1^+$	964.41(4)	100.0(3)	2039.08
3388.4(1)	$5^- \rightarrow 3^-$	870.2(2)	24(3)	2518.2
	$5^- \rightarrow 4_1^+$	1349.3(2)	100(3)	2039.08
3505.1(1)	$(5_1^+) \rightarrow 6_1^+$	501.3(5)	4(1)	3003.5
	$(5_1^+) \rightarrow (3_1^+)$	779.8(3)	100(4)	2725.3
	$(5_1^+) \rightarrow 4_2^+$	1121.4(5)	93(7)	2384.0
	$(5_1^+) \rightarrow 4_1^+$	1466.6(4)	45(4)	2039.08
3524.2(1)	$5^- \rightarrow 3^-$	1006.0(1)	33(3)	2518.2
	$5^- \rightarrow 4_2^+$	1140.3(2)	18(4)	2384.0
	$5^- \rightarrow 4_1^+$	1485.1(1)	100(3)	2039.08
3648.7(1)	$6_2^+ \rightarrow 4_2^+$	1264.7(2)	100(10)	2384.0
	$6_2^+ \rightarrow 4_1^+$	1609.7(2)	60(10)	2039.08
3788.7(1)	$6^- \rightarrow 5^-$	264.6(1)	100	3524.2
3916.3(1)	$7^- \rightarrow 6^-$	127.6(2)	7(2)	3788.7
	$7^- \rightarrow 5^-$	527.8(4)	16(2)	3388.4
	$7^- \rightarrow 6_1^+$	912.7(1)	100(3)	3003.5
3945.5(2)	$6_3^+ \rightarrow 4_2^+$	1561.5(2)	100	2384.0
4037.8(1)	$8_1^+ \rightarrow 6_1^+$	1034.30(5)	100	3003.5
4221.6(2)[a]	$(7^-) \rightarrow 6^-$	433.1(3)	–	3788.7
	$(7^-) \rightarrow 5^-$	697.4(2)	–	3524.2
4325.9(1)	$7^- \rightarrow 5^-$	937.5(2)	100(6)	3388.4
	$7^- \rightarrow 6_1^+$	1322.2(2)	80(6)	3003.5
4345.2(1)	$(7_1^+) \rightarrow (5_1^+)$	840.1(1)	100(2)	3505.1
	$(7_1^+) \rightarrow 6_1^+$	1341.7(1)	37(2)	3003.5
4411.7(1)	$(7^-) \rightarrow 7^-$	495.4(1)	100(3)	3916.3
	$(7^-) \rightarrow 6^-$	623.1(2)	8(3)	3788.7
4576.6(2)[a]	$(8^-) \rightarrow 7^-$	660.4(2)	–	3916.3
	$(8^-) \rightarrow 6^-$	787.9(2)	–	3788.7
4607.1(1)	$8_2^+ \rightarrow 8_1^+$	569.3(2)	96(6)	4037.8
	$8_2^+ \rightarrow 7^-$	690.7(2)	100(6)	3916.3
	$8_2^+ \rightarrow 6_2^+$	958.6(3)	85(12)	3648.7
4752.6(1)	$8_3^+ \rightarrow 6_3^+$	807.2(3)	46(11)	3945.5
	$8_3^+ \rightarrow 6_2^+$	1103.8(2)	100(10)	3648.7
	$8_3^+ \rightarrow 6_1^+$	1749.2(2)	85(9)	3003.5
4900.1(1)	$(8^-) \rightarrow (7^-)$	488.3(1)	33(4)	4411.7
	$(8^-) \rightarrow 7^-$	984.0(2)	100(5)	3916.3
	$(8^-) \rightarrow 6^-$	1111.4(1)	20(4)	3788.7
5048.3(2)[a]	$(8^-) \rightarrow 6^-$	1259.4(3)	–	3788.7
5145.4(2)[a]	$(9^-) \rightarrow (8^-)$	245.1(3)	–	4900.1
	$(9^-) \rightarrow (8^-)$	569(1)	–	4576.6
	$(9^-) \rightarrow (7^-)$	923.8(2)	–	4221.6
5207.4(1)	$10_1^+ \rightarrow 8_1^+$	1169.62(7)	100	4037.8
5210.0(1)	$9^- \rightarrow 7^-$	884.0(2)	32(4)	4325.9
	$9^- \rightarrow 8_1^+$	1172.2(5)	11(4)	4037.8
	$9^- \rightarrow 7^-$	1293.8(1)	100(5)	3916.3
5288.0(2)[a]	$(9^-) \rightarrow (8^-)$	387.9(2)	–	4900.1
	$(9^-) \rightarrow 7^-$	1371.7(2)	–	3916.3
5294.4(2)[a]	$(9^-) \rightarrow (8^-)$	394.3(2)	–	4900.1
5319.8(1)	$(9_1^+) \rightarrow (7_1^+)$	974.6(1)	100(4)	4345.2
	$(9_1^+) \rightarrow 8_1^+$	1282.0(1)	14(2)	4037.8
5695.8(2)	$10_2^+ \rightarrow 8_2^+$	1088.4(4)	100(3)	4607.1
	$10_2^+ \rightarrow 8_1^+$	1658.0(2)	55(3)	4037.8
5866.9(2)	$(10_3^+) \rightarrow 10_1^+$	659.5(2)	26(6)	5207.4
	$(10_3^+) \rightarrow 8_3^+$	1114.4(5)	100(7)	4752.6
	$(10_3^+) \rightarrow 8_1^+$	1829.1(2)	40(6)	4037.8
6181.3(2)[a]	$(10^-) \rightarrow (9^-)$	886.9(3)	–	5294.4
	$(10^-) \rightarrow (9^-)$	893.3(3)	–	5288.0
	$(10^-) \rightarrow (9^-)$	1035.9(3)	–	5145.4
	$(10^-) \rightarrow (8^-)$	1132.8(3)	–	5048.3
	$(10^-) \rightarrow (8^-)$	1281.4(3)	–	4900.1
6440.5(3)[a]	$(11_1^+) \rightarrow (9_1^+)$	1120.9(3)	100	5319.8
6491.7(2)	$11^- \rightarrow 9^-$	1281.6(2)	100	5210.0
6512.3(1)	$12_1^+ \rightarrow 10_1^+$	1304.94(7)	100	5207.4
6721.3(1)[a]	$(11_2^+) \rightarrow (9_1^+)$	1401.5(1)	100	5319.8
6961.1(2)	$12_2^+ \rightarrow 10_2^+$	1265.0(5)	100(10)	5695.8
	$12_2^+ \rightarrow 10_1^+$	1753.7(5)	19(8)	5207.4
7110.0(2)	$(12_3^+) \rightarrow (10_3^+)$	1243.1(2)	100(4)	5866.9
	$(12_3^+) \rightarrow 10_1^+$	1902.6(8)	8(4)	5207.4
7251.5(4)[a]	$(12^-) \rightarrow (10^-)$	1070.2(3)	–	6181.3
7309.5(2)	$13^- \rightarrow (12_3^+)$	199.6(2)	21(2)	7110.0
	$13^- \rightarrow 12_2^+$	348.4(2)	28(2)	6961.1
	$13^- \rightarrow 12_1^+$	797.2(2)	100(3)	6512.3
	$13^- \rightarrow 11^-$	817.8(3)	16(2)	6491.7
7613.7(3)	$(13_1^+) \rightarrow (11_2^+)$	892.2(3)	53(9)	6721.3
	$(13_1^+) \rightarrow (11_1^+)$	1173.3(2)	100(9)	6440.5
7709.4(3)	$13^- \rightarrow 11^-$	1217.7(2)	100	6491.7
7944.6(5)	$14_1^+ \rightarrow 12_1^+$	1432.4(6)	100	6512.3
8162.2(5)[a]	$(14^-) \rightarrow (12^-)$	910.7(4)	–	7251.5
8322.8(3)	$14_2^+ \rightarrow 12_2^+$	1361.6(3)	100(5)	6961.1
	$14_2^+ \rightarrow 12_1^+$	1810.6(4)	25(5)	6512.3
8354.1(3)	$15^- \rightarrow 13^-$	1044.6(2)	100	7309.5
8773.8(4)	$15^- \rightarrow 13^-$	1064.4(3)	100	7709.4
9439.0(4)	$16^+ \rightarrow 14_2^+$	1116.1(4)	100(15)	8322.8
	$16^+ \rightarrow 14_1^+$	1494.5(5)	63(15)	7944.6
9481.9(5)	$17^- \rightarrow 15^-$	1127.8(4)	100	8354.1
10659(1)	$18^+ \rightarrow 16^+$	1220.0(5)	100	9439.0

[a]Level tentative due to uncertain γ-ray placement.

to the yrast band. The 5320-keV state is fed by two parallel cascades of 892 + 1420 keV and 1173 + 1121 keV, assumed to be originating from a single state at 7614 keV. As the order of the cascades cannot be confidently determined, the intermediate states at 6721 and 6441 keV are uncertain. The new band is assigned a positive parity, as it does not feed

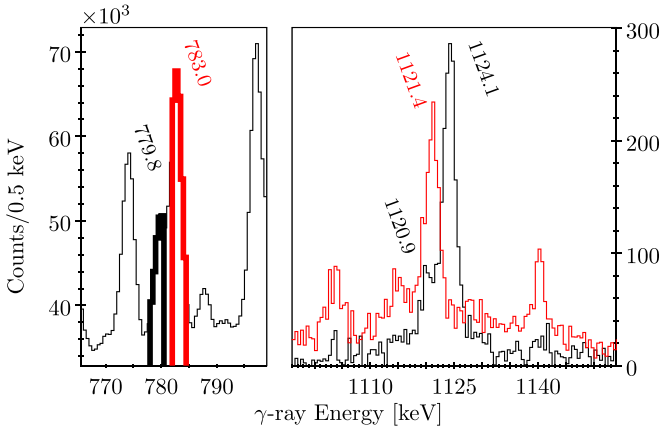

FIG. 4. Gamma-ray spectra from a $\gamma\gamma$ matrix, in coincidence with evaporated α particles in the downstream silicon detector. Two precise gates on the ≈780-keV doublet of the ^{70}Se (2_2^+) band are shown in red and black on the matrix projection (left). The resultant gated spectra showing the partial separation of the ≈1120-keV triplet are shown in red and black color matching the respective gate (right).

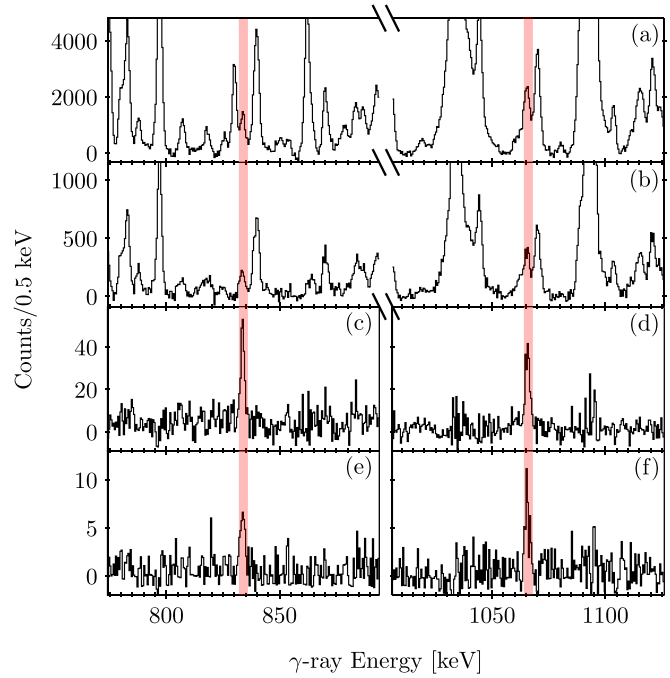

FIG. 5. Gamma-ray energy spectra showing the 1066 and 834 keV γ rays from ^{70}Se, depopulating the 0_2^+ and 2_3^+ states, respectively. Spectra are shown for a 945-keV gate on the $\gamma\gamma$ (a) and the α-coincident $\gamma\gamma$ (b) matrices, a 945+1066 keV double gate on the $\gamma\gamma\gamma$ (c) and α-coincident $\gamma\gamma\gamma$ (e) matrices, and a 945+834 keV double gate on the $\gamma\gamma\gamma$ (d) and α-coincident $\gamma\gamma\gamma$ (f) matrices. The continuity of the 834 and 1066 keV peaks in the relevant spectra is highlight by bands to guide the eye.

any of the previously identified negative-parity states. Furthermore, it is suggested that these new states form an odd-spin band starting from the 2725-keV (3^+) state. An alternative assignment of 4_3^+ for the 2725-keV state is allowable, but this would leave ^{70}Se without a clear 3^+ candidate, as identified in neighboring nuclei. Based on the branching ratio, the 3505-keV state, and the states above it, are more strongly connected to the 2725-keV state and do not form a band above the 2384-keV 4_2^+ state. It was not possible to determine γ-ray angular correlations to confirm this assignment with the present data.

The 3649-keV 6_2^+ state which feeds the 4_2^+ state was identified. An additional 1610-keV $6_2^+ \rightarrow 4_1^+$ branch was confirmed, as previously reported in Ref. [40] and also observed in [41,42] but erroneously assigned to a spurious 2553-keV 4^+ state. An additional 959-keV $8_2^+ \rightarrow 6_2^+$ transition, reported in [40,43,44], is also observed, connecting the 6_2^+ to higher spin band members. It was not possible to observe the 661- and 1603-keV transitions from this 8_2^+ state which have been previously reported [39,40]. The determined $B(E2; 6_2^+ \rightarrow 4_2^+)/B(E2; 6_2^+ \rightarrow 4_1^+)$ ratio is 5.6, supporting positioning the 4_2^+ state, and subsequently the 2_2^+ state, in a band beneath the 3649-keV 6_2^+ state.

We confirm an additional 6_3^+ state at 3945 keV, which depopulates via a 1562-keV transition to the 4_2^+ state. When first reported in Ref. [40], the exact placement of the 6_3^+ state was uncertain, but it is now confirmed by the observation of an additional 807-keV feeding transition from the 8_3^+ state at 4753 keV, which is also confirmed here. The $B(E2; 8_3^+ \rightarrow 6_3^+)/B(E2; 8_3^+ \rightarrow 6_2^+)$ ratio of 2.2 shows the new transition to the 6_3^+ state to be favored with energy weighting removed. In addition, a (10_3^+) state at 5867 keV and a (12_3^+) state at 7110 keV are newly reported, identified by both a cascade to the 8_3^+ state and decay branches to the yrast band. The (12_3^+) state is further verified by a new 200-keV transition from the 7310-keV 13^- state.

In coincidence with an observed 1066-keV transition, which originates from a 2011-keV state with a previous tentative (0^+) assignment [45], a new transition is identified at 834 keV, see Fig. 5, which is attributed to a (2_3^+) state placed at 2845 keV. No additional transitions linking either of these states were identified.

2. Negative-parity states

The negative-parity yrast band based on the 2518-keV 3^- state was populated up to the 8774-keV 15^- state. However, based on the relative intensities observed in this study, the ordering of the $15^- \rightarrow 11^-$ 1218- and 1064-keV cascade is reversed from previous reports [41], placing the 13^- state at 7709 keV. Two new γ-ray branches from the 5210-keV 9^- state were found, with energies 884 and 1172 keV.

Two additional transitions depopulating the 7310-keV 13^- state were identified feeding the new 7110-keV (12_3^+) state and the 6492-keV 11^- state. Due to its lifetime of 2.3(3) ns, the 7310-keV state was previously assigned as 13^- [41], despite only feeding 12^+ states in previous level schemes. The new transition to the 11^- state further constrains the spin parity; however, the $E1$ transitions to the 12^+ states still dominate. Using the previously reported lifetime the reduced transition strengths for the 200-, 348-, 797- and 818-keV transitions can be determined as $B(E1) = 4.0(6) \times$

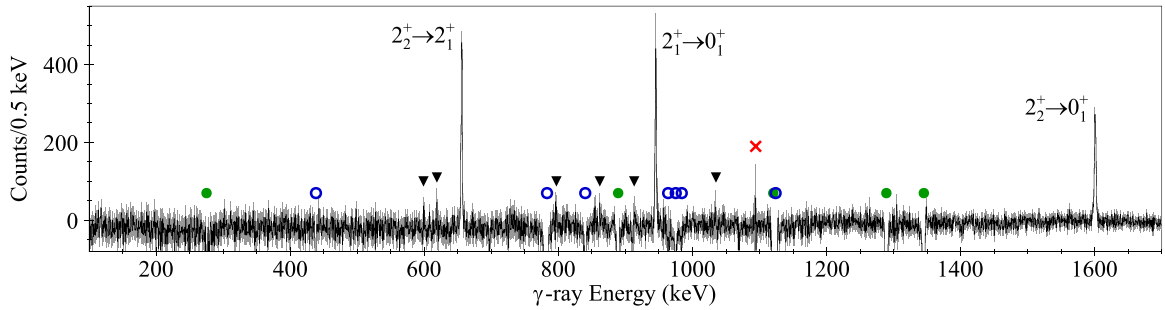

FIG. 6. Spectrum showing transitions depopulating the 1601-keV 2_2^+ state in ^{70}Se, from a gate on the $4_2^+ \rightarrow 2_2^+$ γ ray. Known transitions are labeled. An artefact resulting from Compton subtraction of the intense to $4_1^+ \rightarrow 2_1^+$ transitions is marked with a cross. Remaining positive features, which may correspond to unidentified transitions, are highlighted with triangles. Visibly oversubtracted peaks from ^{70}Se and ^{46}Ti are produced as a result of the procedure described in Sec. III A 3, and are marked with open and closed circles, respectively.

10^{-6} W.u., $B(E1) = 1.1(2) \times 10^{-6}$ W.u., $B(E1) = 3.0(4) \times 10^{-7}$ W.u., and $B(E2) = 0.0055(9)$ W.u., respectively.

Two new feeding transitions to the 3789-keV 6^- state are identified from the states at 4412 and 4900 keV. As these transitions would seem to contradict the previous 9^- assignment [38] for the higher-lying state, spins of 7^- and 8^- are suggested, respectively.

An additional 17 new γ rays were identified feeding the known negative-parity states. Due to the limited statistics, and many parallel branches, the placement of additional states associated with these transitions is extremely tentative and so branching ratios are not reported. The previously reported [38] band above the 4900-keV negative-parity state was not observed in the present work. Two of the newly placed γ rays (1070 and 911 keV) match the energy of previously reported transitions, but with a different arrangement.

3. $2_2^+ \rightarrow 0^+$ *transitions in γ-ray data*

Extensive γ-ray gating was performed specifically in order to identify any γ rays feeding an unidentified 0^+ state in ^{70}Se, particularly from the 1601-keV 2_2^+ state. Figure 6 shows a spectrum of γ rays depopulating the 2_2^+ state. To produce this spectrum, α-particle coincidence was required to preferentially select the channel of interest. A γ-ray spectrum in coincidence with the ^{70}Se $4_2^+ \rightarrow 2_2^+$ 783-keV transition was then selected. From this initially gated spectrum, a subtraction was performed in order to cleanly select only γ rays depopulating the 2_2^+ state, by removing those feeding the 4_2^+ state. The subtraction spectra of populating γ rays was produced by gating on the $2_2^+ \rightarrow 0_1^+$ 1601-keV transition. This subtraction was scaled suitably to remove the known 4_2^+ state feeding transitions from the resultant spectra, shown in Fig. 6. The resultant spectrum contains three clearly identifiable peaks corresponding to the 656-keV $2_2^+ \rightarrow 2_1^+$, 945-keV $2_1^+ \rightarrow 0_1^+$, and 1601-keV $2_2^+ \rightarrow 0_1^+$ transitions in ^{70}Se. Owing to a strong 1598-keV transition from the contaminant ^{46}Ti [produced in the ^{16}O(^{36}Ar, α2p)^{46}Ti reaction], which falls in the gate for the subtraction spectrum, a series of peaks from ^{46}Ti appear over-subtracted in the final spectrum, in addition to expected over-subtracted ^{70}Se peaks. The spectrum contains some artefacts from imperfect subtraction, including a notable feature resulting from the intense ^{70}Se 1094-keV $4_1^+ \rightarrow 2_1^+$ peak, which is removed during standard Compton background subtraction as part of the gating procedure. Following the identification of known spectral elements, multiple small positive features remain. While these do not have either a sufficient width or size to be suitably identified above background as a spectroscopic peak, they could provide evidence in concert with other observations (see Sec. III B 2) but are insufficient to suggest an identification by themselves. Based on $B(E2)$ ratios in neighboring nuclei, it would be expected that a 0_2^+ state below 1200 keV would have feeding γ rays of sufficient intensity to be clearly identified in this spectrum. A transition which is degenerate with one of the observed (or intentionally subtracted) peaks cannot be ruled out; however the FWHM of the 656- and 945-keV peaks are 2.0(1) and 2.4(2) keV, respectively, which is consistent with a solitary peak at those energies in this dataset.

B. Internal conversion electrons

A singles electron spectrum from the SPICE detector is shown in Fig. 7. Broadened peaks from straggling in the thick recoil-catcher foil, combined with many contributing fusion-evaporation channels, result in a singles spectrum

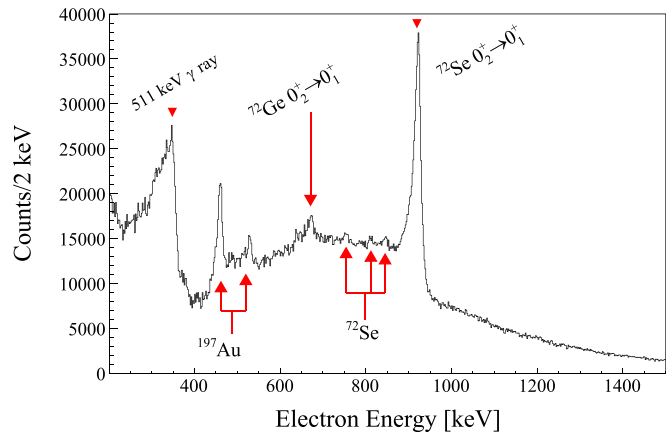

FIG. 7. Raw energy spectrum from the SPICE Si(Li) detector, resulting from SPICE singles trigger events with no coincidence requirement. Notable features are labeled with their origin, see text for details.

where only the strongest features can be clearly identified. ICE peaks can be identified resulting from Coulomb excitation of the gold antioxidation coating of the target, alongside known $E0$ transitions from ^{72}Se and ^{72}Ge, and three $E2$ transitions from the ^{72}Se yrast band. The large feature at 341 keV is the Compton edge from 511-keV γ rays hitting the Si(Li) detector. Buildup of β^+ emitters in the target result in the production of an appreciable quantity of β^+ particles which escape the target and annihilate in the chamber walls. The annihilation photons produced away from the shielded target position can subsequently reach the SPICE detector. With the magnet configuration used in this experiment, the ICE detection efficiency for SPICE drops off rapidly below 500 keV.

1. Isomeric sum-peak analysis

Due to the nature of the fusion-evaporation reaction used to populate ^{70}Se predominantly feeding high spin states, it is anticipated that any 0^+ states would be populated by γ-ray feeding and not directly. While there is currently no clear candidate for a new 0_2^+ state in ^{70}Se, one may propose the existence of a $2_2^+ \rightarrow 0_2^+ \rightarrow 0_1^+$ cascade. It would follow to adopt a procedure similar to Sec. III A 3 by gating on γ rays feeding the 2_2^+ state in order to identify coincident ICEs from the depopulation cascade. Unfortunately, the spectral quality resulting from such a selection is insufficient to identify an unknown-energy transition. However, by considering a spectrum of $E_\gamma + E_{ICE}$, the sum of coincident γ rays and ICEs, one can look for a peak at a known energy corresponding to $E_{2_2^+} - E_{\text{K Binding}}$ (for selenium $E_{\text{K Binding}} = 12.7$ keV). Furthermore, due to the isomeric nature of low-lying 0^+ states, the time difference between the feeding γ-ray and depopulating electron may be used to preferentially select sum peaks from events of interest over background contributions. Figure 8 shows an isomerically gated sum-peak spectrum from this work, selected on a time difference of 10–100 ns. A peak corresponding to the $2_2^+ \rightarrow 0_2^+ \rightarrow 0_1^+$ cascade, which would appear at 1588 keV, is not observed above background. However, by comparing an upper-limit measurement of the cascade sum-peak area, $N(e\gamma)$, to the counts expected based on the observed population of the 2_2^+ state, $N(\gamma\gamma)$, further insight on the probable presence of a low-lying 0_2^+ state is gained. The technique is demonstrated in Fig. 9 for the equivalent observable sum peak in ^{72}Se, where $E(0_2^+)$ is treated as unknown. As detection efficiencies and $\tau(0_2^+)$, detailed below, depends on $E(0_2^+)$, the gating conditions and corrections applied result in a sum-peak count $N(e\gamma)$ which varies with energy. The location at which the two experimental bands of expected and observed counts intersect provides the experimental result for $E(0_2^+)$. In this case of ^{72}Se the intersection agrees well with the literature value of 937 keV, thus validating the power of this analysis technique.

Figure 10 demonstrates the potential decay paths for the depopulation of the 2_2^+ state in ^{70}Se and introduces the index notation used in the following section. The lifetime of the 0_2^+ state is given by

$$\tau = \frac{1}{\lambda_\gamma(E2)(1+\alpha_{\text{tot}}) + \lambda(E0)}, \qquad (1)$$

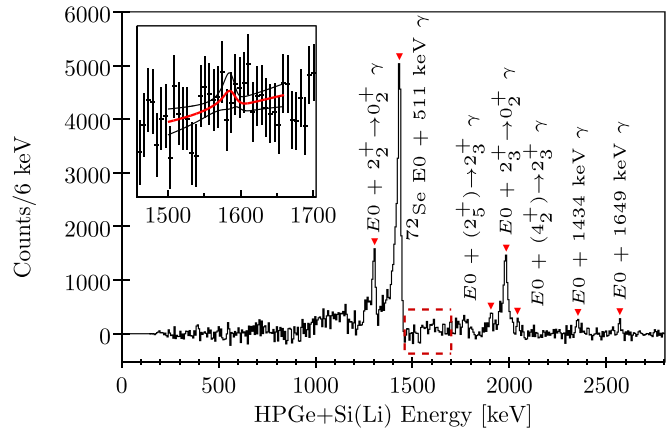

FIG. 8. Sum spectrum of γ rays detected in TIGRESS and ICE detected in SPICE, selected for a $\gamma - e^-$ time difference of 10–100 ns. A background subtraction of prompt events and of an interpolated continuum background has been performed. The peaks observed correspond to the combination of the ^{72}Se 937-keV $0_2^+ \rightarrow 0_1^+$ transition [$\tau(0_2^+) = 27.6\,(3)$ ns] summed with various γ rays, most notably a 511-keV annihilation photon from the β decay of ^{72}Br. The inset shows an expanded view of the region corresponding to a possible sum peak from depopulation of the ^{70}Se 2_2^+ state. A constrained fit with uncertainty bands is shown; it is consistent with zero counts within 1σ.

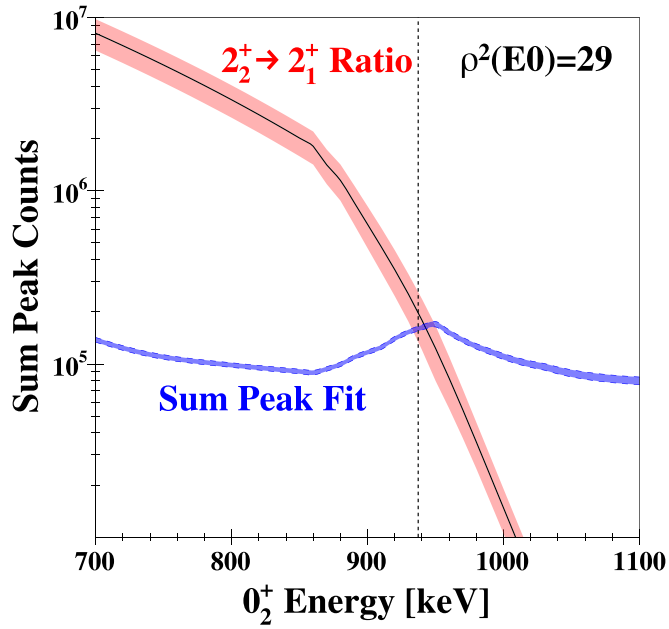

FIG. 9. Measured counts for the γe^- sum peak from ^{72}Se $2_2^+ \rightarrow 0_2^+ \rightarrow 0_1^+$ cascade events $N(e\gamma)$ (blue dashed), plotted as a function of $E(0_2^+)$, which is treated as unknown in this example. The count varies with energy due to corrections for $\tau(0_2^+)$ which depend on $E(0_2^+)$. The number of expected γe^- cascade events, calculated from the observed $2_2^+ \rightarrow 2_1^+$ intensity and known $\rho^2(E0)$ value, $N(\gamma\gamma)$, is overlain (red band). The location at which the bands of expected and observed counts intersect agrees well with the literature value of $E(0_2^+) = 937$ keV, represented by the dotted black line.

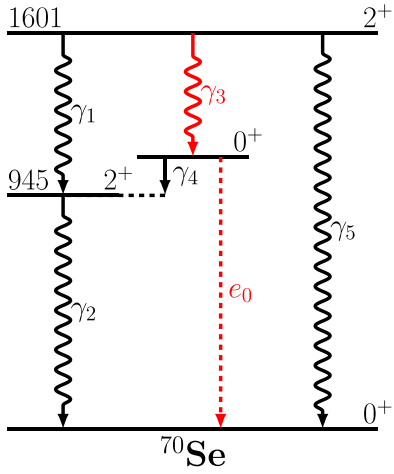

FIG. 10. ^{70}Se 2_2^+ state hypothetical decay paths. The transitions highlighted in red correspond to the expected sum peak.

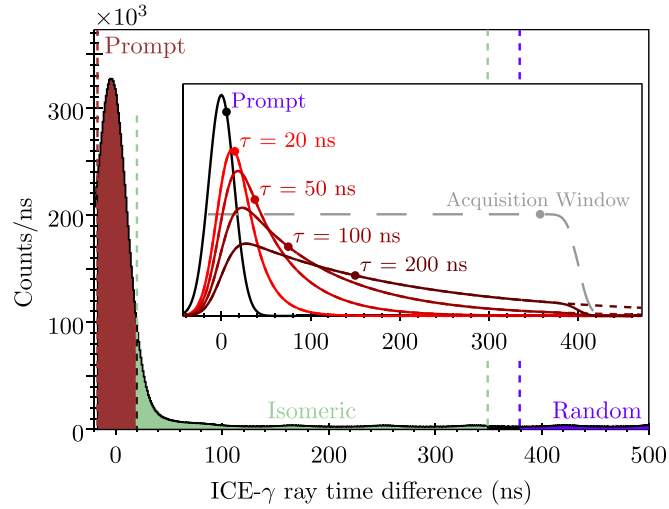

FIG. 11. Illustration of the components of the isomeric time gating performed in ICE+γ ray sum-peak analysis. The main histogram shows the time difference between all coincident ICE and γ rays from the experimental data, overlain with the time gates used for sum-peak measurement when $\tau = 100$ ns. The inset shows the idealized distributions for different lifetimes; this does not include the E_γ-dependent tail, which is determined from data and corrected for in the analysis. The experimental acquisition window extends to Δt=1000 ns but is shown reduced here for illustrative purposes.

in which the decay constants $\lambda_\gamma(E2)$ and $\lambda(E0)$, and $\alpha_{\rm tot}$, the γ_4 total conversion coefficient, depend on the undefined state energy. Additionally, to determine the decay constants, reasonable values of transition strengths $B(E2)$ and $\rho^2(E0)$ must be assumed. We take the value of $B(E2;0_2^+\rightarrow 2_1^+) = 148(5)$ W.u. from neighboring ^{72}Se [35] and produce plots for a range of $\rho^2(E0)$ values.

Each value of $E(0_2^+)$ will have a different time distribution due to changing $\tau(0_2^+)$, and γ-ray tailing dependent on E_{γ_3}. Subsequently, gates for isomeric events, as well as time-random and prompt background subtraction spectra, must be optimized, as demonstrated in Fig. 11. The amount of isomeric events falling within the gates will vary, and this must be corrected. For example, of the time gates for $\tau = 100$ ns, shown in Fig. 11, 68% of isomeric events are within the gating window. Also, while 18% of the isomeric distribution falls within the prompt background gate, only 2.8% of the prompt peak falls in the isomeric window. Hence, the prompt subtraction scaling factor is very small (0.08). After adjusting for counts removed by both background subtractions, the area determined for this example would equate to 66.4% of the total isomeric peak.[1] This correction can be represented by the formula

$$N(e\gamma)_{\rm Corr.} = N(e\gamma)_{\rm Fit}/\left(F_{ig} - F_{pg}R_p - F_{rg}R_r\right), \qquad (2)$$

where $N(e\gamma)_{\rm Fit}$ is the area determined from a fit to the background-subtracted spectrum, F_{ig}, F_{pg}, and F_{rg} are the fractions of isomeric events falling in the isomeric, prompt, and random time gates, respectively, while R_p and while R_r are the ratios for the relative amounts of each background falling inside the isomeric and respective background gates. For the shortest lifetimes gates, in which a spectral subtraction of prompt background is not possible, the contribution from internal conversion of the $(\gamma_1\gamma_2)$ decay path was instead calculated from the observed γ-ray intensity.

A comparison can then be made between $N(e\gamma)$ determined from sum-peak measurement and that expected from the observed 2_2^+ state population, $N(\gamma\gamma)$, which is given by

$$N(\gamma\gamma) = N_{\gamma_1}B_{3,1}/(1 + B_{4,0}), \qquad (3)$$

in which $B_{4,0} = I_{\gamma_4}/I_{e_0}$ is the branching ratio for depopulation of the 0_2^+ state, which depends on the assumed decay strengths determined for Eq. (1). N_{γ_1} is the efficiency-corrected counts for the $2_2^+\rightarrow 2_1^+\rightarrow 0_1^+$ $(\gamma_1\gamma_2)$ branch, which must be used to determine population rather than the direct $2_2^+\rightarrow 0_1^+$ (γ_5) decay, due to the data acquisition system (DAQ) configuration rejecting multiplicity 1 γ-ray events. The branching ratio $B_{3,1} = I_{\gamma_3}/I_{\gamma_1}$ is determined by energy scaling an adopted $B(E2)_{\gamma_3}/B(E2)_{\gamma_5}$ ratio and multiplying by the experimentally measured ^{70}Se $I_{\gamma_5}/I_{\gamma_1}$ ratio. The $B(E2)$ ratio from neighboring ^{72}Se is 81(10) [35], and for neighboring ^{68}Ge it is 150(70) [46]. The ratio may also be taken from ^{70}Se itself by assuming an equivalence of the $\Delta L = 2$ inter- and intraband matrix elements of 4_2^+ and 2_2^+ states, yielding a value of 30(3). An unweighted average value with inflated uncertainty of 90(60) is used.

Figure 12 shows the expected counts for the ^{70}Se sum peaks, $N(\gamma\gamma)$, as a function of $E(0_2^+)$ for different values of $\rho^2(E0)$. Overlain is the upper limit for the number of counts in the sum peak deduced from the experimental sum spectrum, $N(e\gamma)$, which has been corrected for lifetime and detection efficiency at each point. Statistical error bands for the expected counts are shown which include an inflated 50% uncertainty on assumed $B(E2)$ values.

[1]The prompt background subtraction also removes some time random background. This is accounted for when determining the subtraction fraction for the time random background.

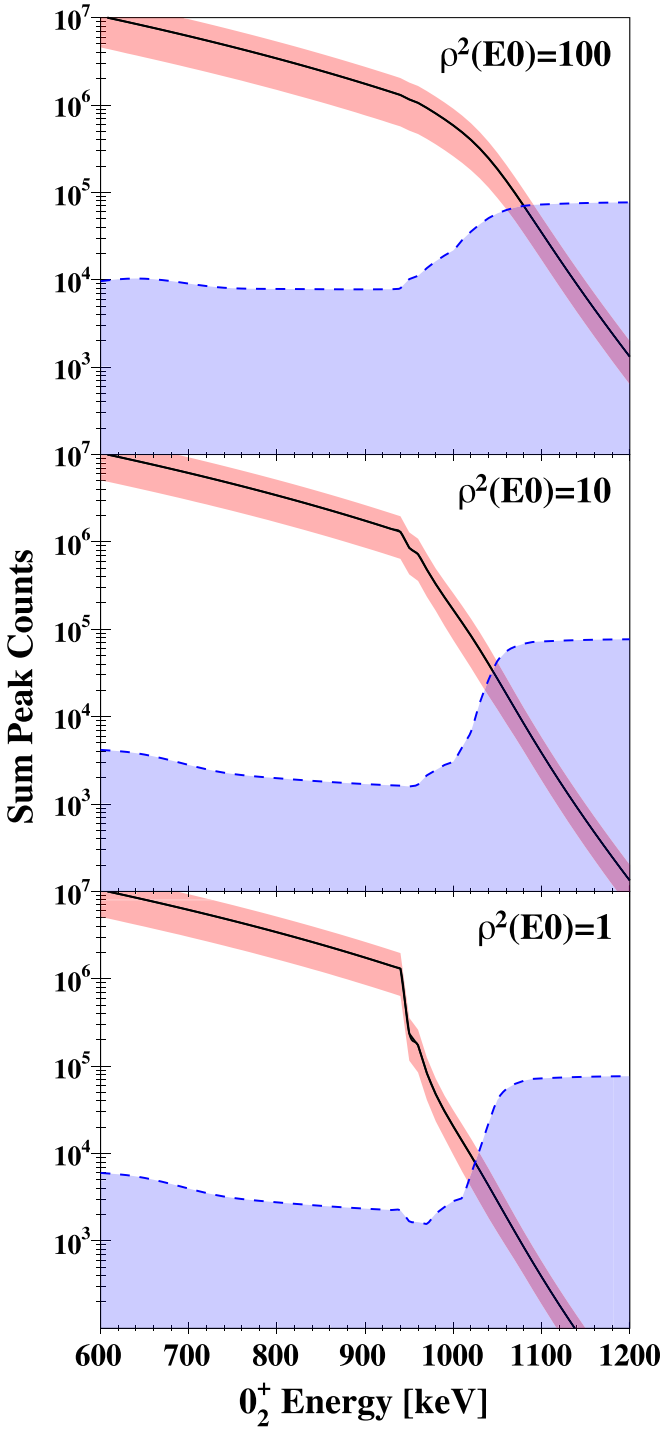

FIG. 12. The total number of $2_2^+ \rightarrow 0_2^+ \rightarrow 0_1^+$ cascade events expected for ^{70}Se, based on the observed $2_2^+ \rightarrow 2_1^+$ γ-ray intensity and assumed branching ratios, $N(\gamma\gamma)$ (solid red), shown as a function of $E(0_2^+)$ for various $\rho^2(E0)$ strengths in milliunits. The upper limit of counts in the sum peak deduced directly from the experimental sum spectrum, $N(e\gamma)$, is overlain (blue dashed).

It can clearly be seen that irrespective of $E0$ strength, below ≈1000 keV the upper-limit measurement determined from the experimental data ostensibly rules out any possible 0^+ state. At higher energies, as the lifetime of the states becomes very short, the expected sum peak is overwhelmed by prompt background contributions and no conclusions can be drawn.

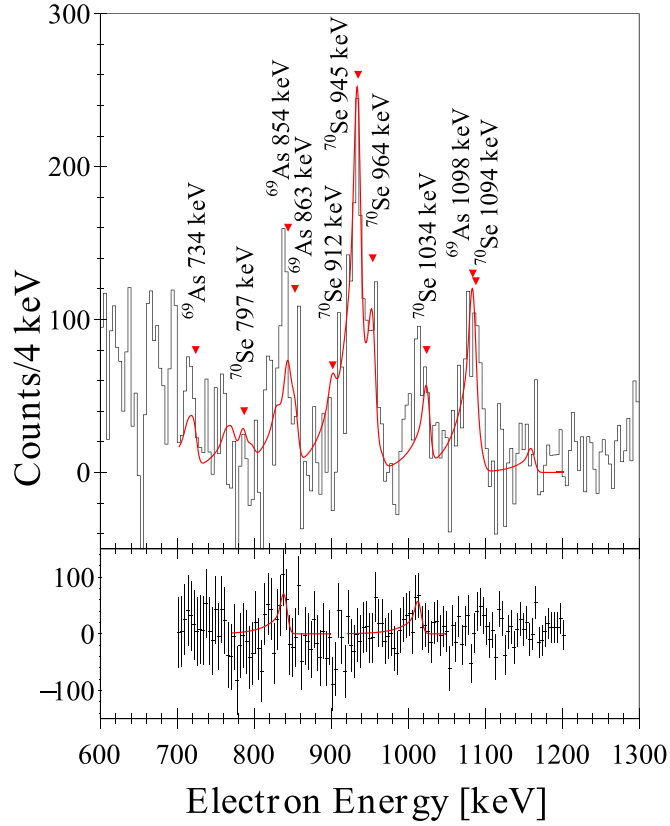

FIG. 13. (Top) Fit to the α-particle-coincident SPICE spectrum constraining all known ICE peaks, relative to the observed counts of their counterpart γ rays, through their respective internal conversion coefficients and detection efficiencies. The ten largest contributions are indicated with the isotope of origin and transition energy. (Bottom) Residuals following subtraction of constrained fit shown in top panel. Fits to two remaining positive features, using constrained shape parameters, are shown.

2. *Evaporation particle-coincident ICE*

In the case of a short-lived 0^+ state (<20 ns), it may still be possible to identify a $0^+ \rightarrow 0^+$ transition by coincidence with an ejectile particle of the production reaction, even when there is no feeding γ ray. In the case of ^{70}Se and the reaction ^{40}Ca(^{36}Ar, α2p) ^{70}Se, an α particle most cleanly selects the nucleus of interest. Figure 13 shows the spectrum observed in SPICE coincident with α particles. A subtraction of smooth continuum background has been performed to highlight the structures of interest. In order to separate any $E0$ peak of interest from the internal conversion components of known transitions, the α-coincident γ-ray spectrum was fit to determine the intensities of known transitions. Using the relative detection efficiencies for γ rays and electrons, together with the calculated ICC from BrIcc [47], the expected size of ICE peaks from known transitions were calculated. A total of 60 transitions were included from ^{70}Se, ^{67,69}As, ^{71}Br, ^{43}Sc,

^{46}Ti, and ^{47}V. The ICE peak shapes and shifted position, due to energy loss in the thick target foil, were determined from the γ-gated electron fits used in construction of the in-beam efficiency curve [35]. By applying these constraints, a fit was made to the α-coincident electron spectra, shown in Fig. 13. The resultant curve was subtracted to leave only unknown electron features. Two prominent features remain in the residual spectrum. Fitting to these features, with the same constrained electron peak-shape parameters, gave energies of 840(10) keV and 1010(10) keV. The fits yield a greater than 90% probability, using a Pearson's chi-squared test, that these additional features, which have not been accounted for by known transitions observed in the γ-ray data, are real and not background fluctuations. However, it cannot be conclusively determined from this dataset that these are peaks from $E0$ transitions, or indeed originate from ^{70}Se. The counterpart $2_2^+ \rightarrow 0_2^+$ γ-ray energies of 750(10) and 580(10) keV do not corresponding to any of features observed in Fig. 6.

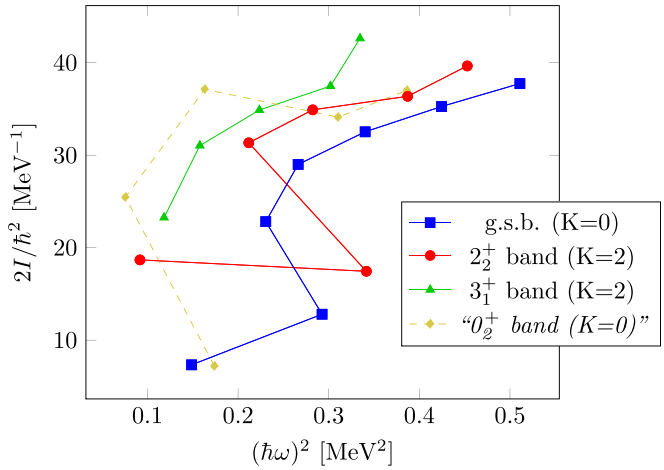

FIG. 14. Moment of inertia plots for the identified bands in ^{70}Se using assumed K values.

3. Decay of 2011-keV (0^+) state

Gamma rays depopulating the known (0_2^+) state at 2011 keV were observed at 1066 keV, as expected for the $(0_2^+) \rightarrow 2_1^+$ transition, following a coincidence requirement with the $2_1^+ \rightarrow 0_1^+$ γ ray. To further clean the spectrum, a background from a $4_1^+ \rightarrow 2_1^+$ gate was subtracted. A peak area of $1.3(3) \times 10^3$ was observed, corresponding to a population level 0.018(5) times that of the 4_1^+ state. Comparison to the population of the 2_1^+ state is not possible due to the DAQ triggering conditions. Owing to the high energy of the state and the competing γ-ray branch, an electron peak is not observed for the $(0_2^+) \rightarrow 0_1^+$ transition. An upper-limit fit to the electron spectrum was performed, but due to the high background a relatively meaningless $q_K^2(E0/E2) < 13$ is determined; the real value is estimated to be at least 1000 times smaller. Lack of a known lifetime prevents comment on the possible $\rho^2(E0)$ strength.

IV. DISCUSSION

In this work, highly tentative $E0$ transition candidates were identified which would, after correction for electron binding energy, correspond to 0^+ states in ^{70}Se at 850(10) and 1020(10) keV. By assuming equivalent $B(E2)$s to neighboring isotopes, as discussed in Sec. III B 1, a branching ratio of γ rays $I(2_2^+ \rightarrow 0_2^+)/I(2_2^+ \rightarrow 0_1^+)$ of 1.8 and 0.5, respectively, would be anticipated for feeding of a 0^+ state at these energies. Such γ-ray transitions were not observed in the present work. The present experiment is, however, insensitive to a longer-lived 0^+ state (>20 ns) which lacks γ-ray feeding.

In Ref. [40], Morales *et al.* found no γ rays within 800 ns of the β decay of the ^{70}Br $T = 1\,0^+$ state. It was assumed this decay exclusively feeds the ^{70}Se ground state. While this does not rule out the presence of a very low-lying 0^+ state decaying exclusively by internal conversion, it does show that the known 2011-keV (0_2^+) state in ^{70}Se has little overlap with the ^{70}Br ground-state wave function, perhaps indicating an intruder configuration of different shape. Furthermore, in the recent report of population using a nucleon removal reaction [21], there was no evidence found for a low-lying 0^+ state in ^{70}Se. Such reactions would be expected to be an effective means of populating multi-particle–multi-hole excitations consistent with the shell-model picture of shape coexistence. Recent Excited Vampir beyond-mean-field model calculations [48] predict near maximally mixed coexisting oblate-prolate states in ^{70}Se. The calculations reproduce the energies of the $2_{1,2,3}^+$ states well and place the 0_2^+ state at approximately 1.6 MeV.

The combined experimental evidence strongly suggests that the lowest-lying excited 0^+ state in ^{70}Se is the known 2011-keV state. In the case of the crossing of oblate and prolate coexisting bands, the crossing point of the bands, where the lowest (0_2^+) state is observed, would then be between ^{72}Se and ^{74}Se. This would imply a series of crossing points located at decreasing values of N for successive elements; with band crossings at $^{\sim 72}_{32}\mathrm{Ge}_{\sim 40}$, $^{\sim 73}_{34}\mathrm{Se}_{\sim 39}$, and $^{\sim 74}_{36}\mathrm{Kr}_{\sim 38}$. Such an interpretation would appear to be in disagreement with Coulomb excitation results [18], which found a negative (prolate) spectroscopic quadrupole moment for the ^{72}Se 2_1^+ state, and suggest a crossing between ^{70}Se and ^{72}Se.

Upon considering the significant changes to the positive-parity-level scheme of ^{70}Se presented here, see Fig. 3, it is prudent to examine the yrast and 2_2^+ bands under the assumption there is no missing 0^+ state. Under this assumption, the 2_2^+ band is taken to be some form of quasi-γ band and assigned a $K = 2$ spin. A moment of inertia plot for the proposed bands is given in Fig. 14. For the lowest spins there are strong discontinuities, particularly around the 2_1^+ and 4_2^+ states, indicating a rapidly changing moment of inertia. Above $J = 6$ the bands show approximately linear trends consistent with a fixed MOI rotor. Included in the plot is a speculative calculation for the identified 0_2^+ band, connected with the 6_3^+ band, which could feasibly be a part of the same structure. There is a significant inflection between the two parts indicating a poor agreement with such a supposition. A 4^+ member would be expected around ≈3300 keV, but there is presently no candidate.

TABLE II. Experimental transition rate and state energy ratios compared to those determined from models.

	Expt.	Davydov Filippov	GTRM	GBH-UNEDF1	
				Unscaled	Scaled
γ (deg)		$27.0\binom{4}{6}^\circ$	$21(9)^\circ$		
Γ (deg)			$-12(7)^\circ$		
$\frac{B(E2;2_2^+\to 0_1^+)}{B(E2;2_1^+\to 0_1^+)}$	0.026(7)	$0.021\binom{8}{5}$		0.080	0.12
$\frac{B(E2;2_2^+\to 2_1^+)}{B(E2;2_1^+\to 0_1^+)}$	0.7(2)	$1.19\binom{6}{10}$		2.0	1.9
$\frac{B(E2;3_1^+\to 2_2^+)}{B(E2;3_1^+\to 2_1^+)}$	50(8)	$48\binom{15}{14}$		11	7.7
$\frac{E(2_2^+)}{E(2_1^+)}$	1.7	$2.15\binom{8}{4}$		1.9	2.0
$\frac{E(3_1^+)}{E(2_1^+)}$	2.8	$3.15\binom{8}{4}$		1.6	1.6

Recent measurements reported a large $\rho^2(E0;2_2^+\to 2_1^+)$ strength in ^{74}Se [49]. It was determined that the 2_2^+ state appeared as a band head but was inconsistent with a typical vibrational γ band, proposing instead a scenario of multiple shape coexistence with triaxiality.

To consider the degree of static triaxiality in ^{70}Se, the low-lying 2_1^+, 2_2^+, and 3_1^+ can be compared to nonaxial rotor calculations of Davydov and Filippov [50]. A χ^2 fit to model-predicted ratios of state energies and $B(E2)$ values was performed as a function of the axial-asymmetry parameter γ; the results are shown in Table II. Energy uncertainties were inflated to 98 keV such that $B(E2)$ and energy ratios contributed equally to the final χ^2, as the greater precision to which state energies can be measured is not a reflection of the degree to which the model describes the data. In order to determine $B(E2)$ values for the decay of the 2_2^+ state, the half-life and δ value from previous works are adopted [39], 3.3(9) ps and $-1.0(\frac{1}{2})$, respectively. The branching ratio measured in the present work is used, which differs significantly from previous reports. Transition strengths of $B(E2;2_2^+\to 2_1^+) = 14(4)$ W.u. and $B(E2;2_2^+\to 0_1^+) = 0.50(14)$ W.u. are deduced. Firstly, in this model, under the assumption these three states are purely rotational, the relationship $E(2_1^+)+E(2_2^+) = E(3_1^+)$ holds true irrespective of the exact value of γ. The ^{70}Se 3_1^+ state deviates 7% from this ideal value. The transition strength ratios show a very good agreement with the model for a near maximal degree of triaxiality of $\gamma = 27.0(5)^\circ$.

The reduced transition strengths of a triaxial nucleus may be better considered in the basis of the generalized triaxial rotor model (GTRM) [51], which improves upon historic model limitations of irrotational flow moments of inertia by treating the inertia tensor and electric quadrupole tensor independently. Within the GTRM the relation of $E2$ matrix elements may be expressed pictorially [52] as

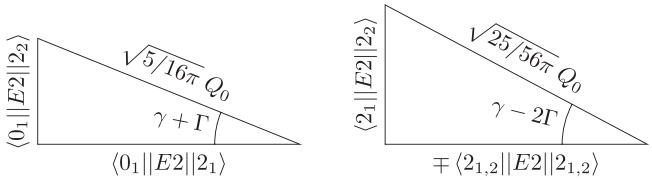

in which γ is the usual "triaxiality angle," while Γ is the "mixing angle" of intrinsic 2^+ states in the model. With a complete set of matrix elements one can test the agreement with the model. However, with the reduced set of 3 available, the remaining parameters can be deduced exactly, without fitting, under the assumption of agreement with the model. Doing so yields a value of $\gamma = 21(9)^\circ$, in reasonable agreement with the Davydov-Filippov model, and $|Q_0| = 1.32(9)$ eb, which is equal to the value one calculates for an axial-symmetric rigid rotor. For both triaxial models, produced results are symmetric about $\gamma = 30^\circ$, only the prolate solutions are presented by convention. Both triaxial calculations show good agreement for a strongly triaxial ground state in ^{70}Se; however, these cannot reproduce the other features of the level scheme, for instance, the 4_2^+ state coming below the 3_1^+ is inconsistent with a pure rotational structure. Furthermore, our application of these models is unable to comment on the softness of the nuclear shape or to any vibrational contributions such softness brings. To fully explore every aspect of the quadrupole deformation space, we turn to the collective generalised Bohr Hamiltonian (GBH) [53]. Following the approach of [54] and [55], the collective generalised Bohr Hamiltonian (GBH) used is of the form

$$\hat{H} = \hat{T}_{\rm vib} + \hat{T}_{\rm rot} + \hat{V}(\beta,\gamma), \tag{4}$$

where

$$\begin{aligned}\hat{T}_{\rm vib} = -\frac{\hbar^2}{2\sqrt{wr}}\Bigg\{ &\frac{1}{\beta^4}\Bigg[\partial_\beta\left(\beta^4\sqrt{\frac{r}{w}}B_{\gamma\gamma}(\beta,\gamma)\right)\partial_\beta \\ &- \partial_\beta\left(\beta^3\sqrt{\frac{r}{w}}B_{\beta\gamma}(\beta,\gamma)\right)\partial_\gamma\Bigg] \\ &+\frac{1}{\beta\sin 3\gamma}\Bigg[-\partial_\gamma\left(\sqrt{\frac{r}{w}}\sin 3\gamma B_{\beta\gamma}(\beta,\gamma)\right)\partial_\beta \\ &+\frac{1}{\beta}\partial_\gamma\left(\sqrt{\frac{r}{w}}\sin 3\gamma B_{\beta\beta}(\beta,\gamma)\right)\partial_\gamma\Bigg]\Bigg\},\end{aligned} \tag{5}$$

$$\hat{T}_{\rm rot} = \frac{1}{2}\sum_{k=1}^{3} I_k^2/J_k, \quad J_k = 4\beta^2 B_k(\beta,\gamma)\sin^2(\gamma - 2k\pi/3), \tag{6}$$

and

$$w = B_{\beta\beta}B_{\gamma\gamma} - B_{\beta\gamma}^2, \quad r = B_1B_2B_3. \tag{7}$$

I_K are the components of angular momentum in the intrinsic frame, J_k are the moments of inertia, and the 6 B functions are the deformation-dependent mass parameters (or inertial functions). The mass parameters were computed by constrained Hartree-Fock-Bogoliubov (HFB) calculations at points across the $\beta\gamma$-deformation space from $\beta = 0-1$ and $\gamma = 0^\circ - 60^\circ$ with a grid size of $\Delta\beta = 0.05$ and $\Delta\gamma = 6^\circ$. There are no free parameters fit to the experimental data, and the calculations are based solely on effective nucleon-nucleon interactions. HFB calculations were conducted in HFODD [56] in 16 shells for UNEDF0 [57], UNEDF1 [58], and UNEDF1SO [59]. Of the results from the subsequent GBH calculations, UNEDF1

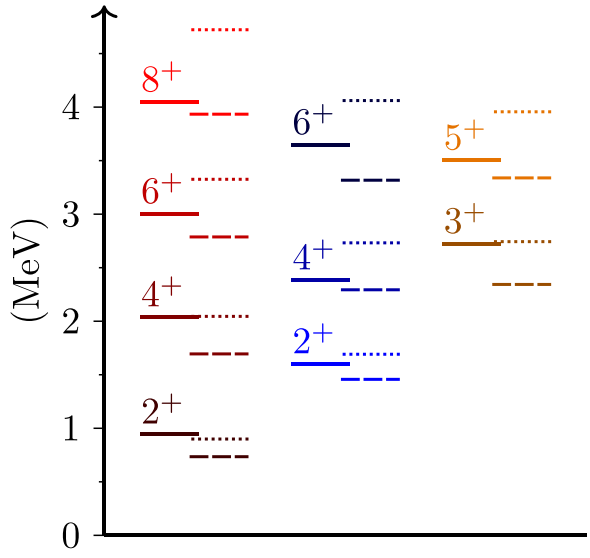

FIG. 15. Comparison of ^{70}Se positive-parity states from experimental results and GBH-UNEDF1 calculations. Experimentally determined energies are given by the solid lines. Calculations from the unscaled Bohr Hamiltonian (BH) are shown as dotted lines, while the BH calculations with scaled mass parameters (1.3) are shown as dashed lines. Corresponding experimental and calculated states are grouped by color.

shows the best agreement with the ^{70}Se experimental data. Mass parameters which enter the Bohr Hamiltonian were calculated using the so-called cranking approximation to the Adiabatic time-dependent HFB theory. In an attempt to account for the missing Thouless-Valatin terms, additional GBH calculations were produced with mass parameters scaled uniformly by a factor of 1.3. The results are presented alongside those using unscaled parameters. Figure 15 shows a comparison of GBH-UNEDF1 predictions and experimental data for low-lying energy levels of ^{70}Se. Remarkable agreement is achieved, with the calculations accurately reproducing the placement and ordering of the new 3_1^+ and 5_1^+ states, as well as the previously known even-spin states. In comparing the calculated and experimental $B(E2)$ values, given in Table III,

TABLE III. Reduced transition strength comparison between experiment and theory. Lifetimes for the calculation of experimental values are taken from Ref. [39].

		GBH-UNEDF1	
	Expt. (W.u.)	Unscaled (W.u.)	Scaled (W.u.)
$B(E2;2_1^+\rightarrow0_1^+)$	19.6(13)	27	23
$B(E2;2_2^+\rightarrow0_1^+)$	0.50(14)	2.1	2.7
$B(E2;2_2^+\rightarrow2_1^+)$	14(4)	54	44
$B(E2;4_1^+\rightarrow2_1^+)$	22(2)	53	45
$B(E2;4_1^+\rightarrow2_2^+)$	13(4)	6.8	3.1
$B(E2;6_1^+\rightarrow4_1^+)$	29(5)	89	71
$B(E2;6_1^+\rightarrow4_2^+)$	12(2)	20	21

there is less impressive agreement, but the qualitative trends of magnitude and branching ratios are approximately reproduced. As the parameters of the model take no input from the experimental data, the limited agreement may still be considered a success. We note that calculated yrast $B(E2)$ values show greater sequential growth, consistent with vibrational behavior, than the experimental values, which show an approximately rotational trend. Calculated GBH wave function probability density distributions for the first few 0^+ and 2^+ states are shown in Fig. 16. Several insights can be gleaned from these calculations. Firstly, a highly triaxial shape is predicted for ^{70}Se, or more accurately, the distribution is very broad, with ^{70}Se effectively having no well-defined shape and showing no strong axial symmetry. This is in agreement with the calculations of Ref. [27]. While the energy of the 0_2^+ state ($\approx$1.5 MeV) does not closely reproduce experiment, it can clearly be seen from the probability density distributions that the 2_3^+ state is the $J = 2$ state associated with that excitation, while the 2_2^+ state, the energy of which is well reproduced, more closely resembles a γ excitation of the ground state.

V. CONCLUSION

In pursuit of a conclusive determination of the shape coexistence situation in selenium isotopes, ^{70}Se was studied by combined γ-ray and internal-conversion-electron spectroscopy. A modified level scheme was constructed and analyzed with comparison to Davydov-Filippov, GTRM, and GBH-UNEDF1 model calculations.

From the γ-ray data, 27 new transitions and eight new states were conclusively identified, alongside additional tentative observations, and confirmation of much of the existing literature. Significant discrepancies were found between the present results and previously reported level schemes. Most notably, the band built upon the 2_2^+ state was found to have been misidentified, and several new positive-parity states were proposed, including odd-spin partners to the 2_2^+ band. No strong evidence for a low-lying 0^+ state was found, despite a careful and thorough search of the γ-ray and electron data. A coexisting state with no significant γ-ray feeding from the populated states could not be ruled out. If a low-lying 0^+ isomer remains undiscovered, the lack of any feeding transitions would need to be explained with additional degrees of freedom outside of the two-shape coexistence model, such as the introduction of destructive interference through inclusion of a third structure.

In an effort to explain the observed states, a comparison of transition strength ratios to triaxial rotor calculations was performed which showed a strong agreement with a near maximally triaxial deformation, within the limits of the rudimentary model. More advanced analysis was provided by GBH-UNEDF1 calculations, which were shown to successfully reproduce the new level scheme. These calculations supported a significantly axial-asymmetric ground state, though without a strongly defined shape. It was determined that these calculations do not support the stance that the 2_2^+ state is part of a coexisting band. Presently it is concluded that the 2_2^+ state corresponds to a quasi-

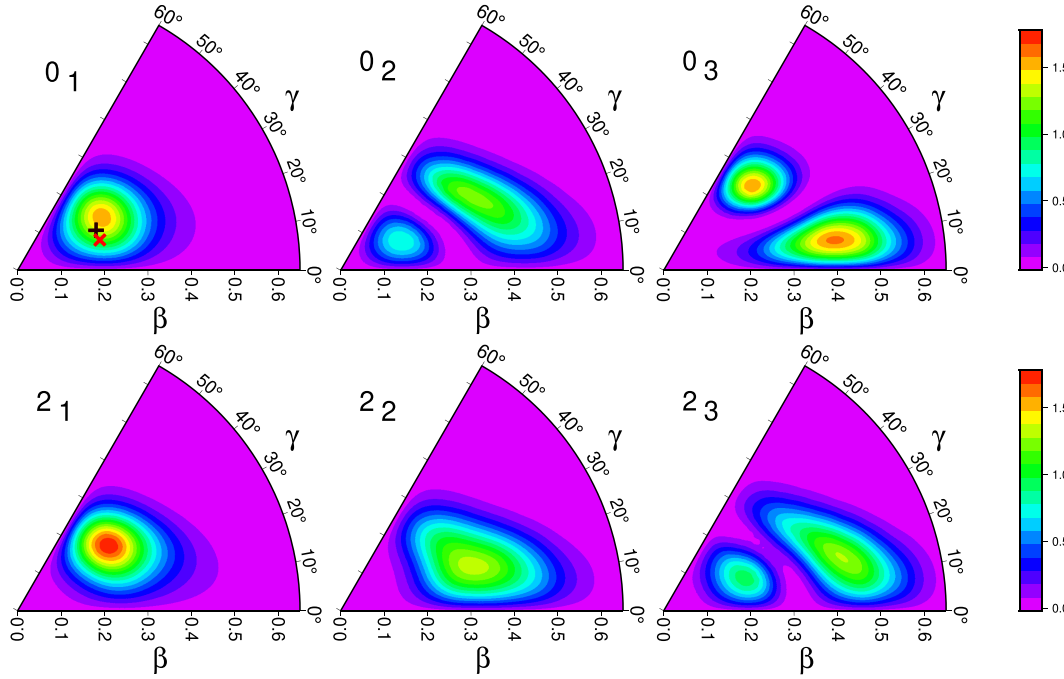

FIG. 16. Wave function probability distributions for the lowest three 0^+ and 2^+ states calculated with GBH-UNEDF1, shown as a function of the quadrupole deformation parameters β and γ. In the first panel, deformation parameters determined for Davydov-Filippov and GTRM are indicated with a plus and cross, respectively.

γ band built on the ground state and not to a coexisting band. Furthermore, it is the conclusion of this work that the present data do not support ^{70}Se as being the crossing point for prolate and oblate coexisting bands in the selenium isotopic chain.

ACKNOWLEDGMENTS

This work was supported by the MEXT Leading Initiative for Excellent Young Researchers, MEXT, Japan Grant No. JPMXS0320210193. Thanks to the beam delivery and technical staff of the TRIUMF-ISAC facility. The SPICE infrastructure was funded by the Canada Foundation for Innovation and the Ontario Ministry of Research and Innovation. TRIUMF receives funding through a contribution agreement through the National Research Council Canada. C.E.S. acknowledges support from the Canada Research Chairs program. This work was supported in part by the Natural Sciences and Engineering Research Council of Canada (NSERC), by U.S. National Science Foundation Grant No. 1606890, and by the Science and Technology Facilities Council (STFC) Grants No. ST/P003885/1 and No. ST/V001035/1.

[1] K. Heyde and J. L. Wood, Rev. Mod. Phys. **83**, 1467 (2011).
[2] J. L. Wood, E. F. Zganjar, C. D. Coster, and K. Heyde, Nucl. Phys. A **651**, 323 (1999).
[3] K. Heyde, J. De Beule, B. Decroix, and C. De Coster, Hyperfine Interact. **127**, 65 (2000).
[4] P. E. Garrett, M. Zielińska, and E. Clément, Prog. Part. Nucl. Phys. **124**, 103931 (2022).
[5] A. Görgen and W. Korten, J. Phys. G: Nucl. Part. Phys. **43**, 024002 (2016).
[6] A. Görgen, J. Phys. G: Nucl. Part. Phys. **37**, 103101 (2010).
[7] F. Becker, W. Korten, F. Hannachi, P. Paris, N. Buforn, C. Chandler, M. Houry, H. Hübel, A. Jansen, Y. Le Coz, C. F. Liang, A. Lopez-Martens, R. Lucas, E. Mergel, P. H., G. Schönwasser, and C. Theisen, Eur. Phys. J. A **4**, 103 (1999).
[8] C. Chandler, P. H. Regan, C. J. Pearson, B. Blank, A. M. Bruce, W. N. Catford, N. Curtis, S. Czajkowski, W. Gelletly, R. Grzywacz, Z. Janas, M. Lewitowicz, C. Marchand, N. A. Orr, R. D. Page, A. Petrovici, A. T. Reed, M. G. Saint-Laurent, S. M. Vincent, R. Wadsworth, Phys. Rev. C **56**, R2924(R) (1997).
[9] S. Chen, P. Doornenbal, A. Obertelli, T. R. Rodríguez, G. Authelet, H. Baba, D. Calvet, F. Château, A. Corsi, A. Delbart, J.-M. Gheller, A. Giganon, A. Gillibert, V. Lapoux, T. Motobayashi, M. Niikura, N. Paul, J.-Y. Roussé, H. Sakurai, C. Santamaria *et al.*, Phys. Rev. C **95**, 041302(R) (2017).
[10] E. Clément, A. Görgen, W. Korten, E. Bouchez, A. Chatillon, J.-P. Delaroche, M. Girod, H. Goutte, A. Hurstel, Y. Le Coz, A. Obertelli, S. Peru, Ch. Theisen, J. N. Wilson, M. Zielinska, C. Andreoiu, F. Becker, P. A. Butler, J. M. Casandjian, W. N. Catford *et al.*, Phys. Rev. C **75**, 054313 (2007).
[11] J. Ljungvall, A. Görgen, M. Girod, J.-P. Delaroche, A. Dewald, C. Dossat, E. Farnea, W. Korten, B. Melon, R. Menegazzo, A. Obertelli, R. Orlandi, P. Petkov, T. Pissulla, S. Siem, R. P. Singh, J. Srebrny, Ch. Theisen, C. A. Ur, J. J. Valiente-Dobón *et al.*, Phys. Rev. Lett. **100**, 102502 (2008).
[12] N. Hinohara, T. Nakatsukasa, M. Matsuo, and K. Matsuyanagi, Phys. Rev. C **80**, 014305 (2009).
[13] W. Andrejtscheff and P. Petkov, Phys. Lett. B **329**, 1 (1994).

[14] S. M. Fischer, C. J. Lister, and D. P. Balamuth, Phys. Rev. C **67**, 064318 (2003).

[15] A. Obertelli, T. Baugher, D. Bazin, S. Boissinot, J.-P. Delaroche, A. Dijon, F. Flavigny, A. Gade, M. Girod, T. Glasmacher, G. F. Grinyer, W. Korten, J. Ljungvall, S. McDaniel, A. Ratkiewicz, B. Sulignano, P. Van Isacker, and D. Weisshaar, Phys. Lett. B **701**, 417 (2011).

[16] Z. Elekes, V. Panin, T. R. Rodrguez, K. Sieja, D. S. Ahn, A. Al-Adili, H. Baba, A. I. Stefanescu, K. J. Cook, Cs. Dósa, N. Fukuda, J. Gao, J. Gibelin, K. I. Hahn, Z. Halász, S. W. Huang, T. Isobe, M. M. Juhász, D. Kim, T. Kobayashi *et al.*, Phys. Lett. B **844**, 138072 (2023).

[17] S. M. Fischer, D. P. Balamuth, P. A. Hausladen, C. J. Lister, M. P. Carpenter, D. Seweryniak, and J. Schwartz, Phys. Rev. Lett. **84**, 4064 (2000).

[18] J. Henderson, C. Y. Wu, J. Ash, P. C. Bender, B. Elman, A. Gade, M. Grinder, H. Iwasaki, E. Kwan, B. Longfellow, T. Mijatović, D. Rhodes, M. Spieker, and D. Weisshaar, Phys. Rev. Lett. **121**, 082502 (2018).

[19] A. M. Hurst, P. A. Butler, D. G. Jenkins, P. Delahaye, F. Wenander, F. Ames, C. J. Barton, T. Behrens, A. Bürger, J. Cederkäll, E. Clément, T. Czosnyka, T. Davinson, G. de Angelis, J. Eberth, A. Ekström, S. Franchoo, G. Georgiev, A. Görgen, R.-D. Herzberg *et al.*, Phys. Rev. Lett. **98**, 072501 (2007).

[20] A. J. Nichols, R. Wadsworth, H. Iwasaki, K. Kaneko, A. Lemasson, G. de Angelis, V. Bader, T. Baugher, D. Bazin, M. Bentley, J. S. Berryman, T. Braunroth, P. J. Davies, A. Dewald, C. Fransen, A. Gade, M. Hackstein, J. Henderson, D. G. Jenkins, D. Miller *et al.*, Phys. Lett. B **733**, 52 (2014).

[21] K. Wimmer, W. Korten, P. Doornenbal, T. Arici, P. Aguilera, A. Algora, T. Ando, H. Baba, B. Blank, A. Boso, S. Chen, A. Corsi, P. Davies, G. de Angelis, G. de France, J.-P. Delaroche, D. T. Doherty, J. Gerl, R. Gernhuser, M. Girod *et al.*, Phys. Rev. Lett. **126**, 072501 (2021).

[22] A. D. Ayangeakaa, R. V. F. Janssens, C. Y. Wu, J. M. Allmond, J. L. Wood, S. Zhu, M. Albers, S. Almaraz-Calderon, B. Bucher, M. P. Carpenter, C. J . Chiara, D. Cline, H. L. Crawford, H. M. David, J. Harker, A. B. Hayes, C. R. Hoffman, B. P. Kay, K. Kolos, A. Korichi *et al.*, Phys. Lett. B **754**, 254 (2016).

[23] J. Henderson, C. Y. Wu, J. Ash, B. A. Brown, P. C. Bender, R. Elder, B. Elman, A. Gade, M. Grinder, H. Iwasaki, B. Longfellow, T. Mijatović, D. Rhodes, M. Spieker, and D. Weisshaar, Phys. Rev. C **99**, 054313 (2019).

[24] A. Mukherjee, S. Bhattacharya, T. Trivedi, R. P. Singh, S. Muralithar, D. Negi, R. Palit, S. Nag, S. Rajbanshi, M. K. Raju, S. Kumar, D. Choudhury, R. Kumar, R. K. Bhowmik, S. C. Pancholi, and A. K. Jain, Phys. Rev. C **105**, 014322 (2022).

[25] H. N. Hady and M. K. Muttalb, J. Phys.: Conf. Ser. **1664**, 012015 (2020).

[26] K. Nomura, R. Rodríguez-Guzmán, and L. M. Robledo, Phys. Rev. C **95**, 064310 (2017).

[27] S. M. Lenzi, A. Poves, and A. O. Macchiavelli, Phys. Rev. C **104**, L031306 (2021).

[28] S. Bhattacharya, T. Trivedi, A. Mukherjee, D. Negi, R. P. Singh, S. Muralithar, S. Jehangir, G. H. Bhat, N. Nazir, J. A. Sheikh, N. Rather, R. Palit, S. Nag, S. Rajbanshi, S. Chakraborty, S. Kumar, M. K. Raju, V. V. Parkar, D. Choudhury, R. Kumar *et al.*, Phys. Rev. C **106**, 044312 (2022).

[29] M. Spieker, L. A. Riley, P. D. Cottle, K. W. Kemper, D. Bazin, S. Biswas, P. J. Farris, A. Gade, T. Ginter, S. Giraud, J. Li, S. Noji, J. Pereira, M. Smith, D. Weisshaar, and R. G. T. Zegers, Phys. Rev. C **106**, 054305 (2022).

[30] A. Ramayya *et al.*, in *Proceedings of the International Conference on Nuclear Structure, Tokyo, September 5-10, 1977*, Journal (Nihon Butsuri Gakkai): Supplement (Physical Society of Japan, Tokyo, 1978), p. 280.

[31] N. Hinohara, K. Sato, T. Nakatsukasa, M. Matsuo, and K. Matsuyanagi, Phys. Rev. C **82**, 064313 (2010).

[32] G. Hackman and C. E. Svensson, Hyperfine Interact. **225**, 241 (2014).

[33] R. E. Laxdal and M. Laxdal, Hyperfine Interact. **225**, 79 (2014).

[34] M. Marchetto and R. E. Laxdal, Hyperfine Interact. **225**, 99 (2014).

[35] J. Smallcombe, A. B. Garnsworthy, W. Korten, P. Singh, F. A. Ali, C. Andreoiu, S. Ansari, G. C. Ball, C. J. Barton, S. S. Bhattacharjee, M. Bowry, R. Caballero-Folch, A. Chester, S. A. Gillespie, G. F. Grinyer, G. Hackman, C. Jones, B. Melon, M. Moukaddam, A. Nannini *et al.*, Phys. Rev. C **106**, 014312 (2022).

[36] M. Moukaddam, J. Smallcombe, L. J. Evitts, A. B. Garnsworthy, C. Andreoiu, G. C. Ball, J. Berean-Dutcher, D. Bishop, C. Bolton, R. Caballero-Folch, M. Constable, D. S. Cross, T. E. Drake, R. Dunlop, P. E. Garrett, S. Georges, G. Hackman, S. Hallam, J. Henderson, R. Henderson *et al.*, Nucl. Instrum. Methods Phys. Res. Sect. A **905**, 180 (2018).

[37] S. Ketelhut, L. J. Evitts, A. B. Garnsworthy, C. Bolton, G. C. Ball, R. Churchman, R. Dunlop, G. Hackman, R. Henderson, M. Moukaddam, E. T. Rand, C. E. Svensson, and J. Witmer, Nucl. Instrum. Methods Phys. Res. Sect. A **753**, 154 (2014).

[38] G. Rainovski, H. Schnare, R. Schwengner, C. Plettner, L. Käubler, F. Dönau, I. Ragnarsson, J. Eberth, T. Steinhardt, O. Thelen, M. Hausmann, A. Jungclaus, K. P. Lieb, A. Müller, G. de Angelis, A. Gadea, D. R. Napoli, A. Algora, D. G. Jenkins, R. Wadsworth *et al.*, J. Phys. G: Nucl. Part. Phys. **28**, 2617 (2002).

[39] G. Gürdal and E. McCutchan, Nucl. Data Sheets **136**, 1 (2016).

[40] A. I. Morales, A. Algora, B. Rubio, K. Kaneko, S. Nishimura, P. Aguilera, S. E. A. Orrigo, F. Molina, G. de Angelis, F. Recchia, G. Kiss, V. H. Phong, J. Wu, D. Nishimura, H. Oikawa, T. Goigoux, J. Giovinazzo, P. Ascher, J. Agramunt, D. S. Ahn *et al.*, Phys. Rev. C **95**, 064327 (2017).

[41] T. Mylaeus, J. Busch, J. Eberth, M. Liebchen, R. Sefzig, S. Skoda, W. Teichert, M. Wiosna, P. von Brentano, K. Schiffer, K. O. Zell, A. V. Ramayya, K. H. Maier, H. Grawe, A. Kluge, and W. Nazarewicz, J. Phys. G: Nucl. Part. Phys. **15**, L135 (1989).

[42] K. Wimmer, W. Korten, T. Arici, P. Doornenbal, P. Aguilera, A. Algora, T. Ando, H. Baba, B. Blank, A. Boso, S. Chen, A. Corsi, P. Davies, G. de Angelis, G. de France, D. T. Doherty, J. Gerl, R. Gernhäuser, D. Jenkins, S. Koyama *et al.*, Phys. Lett. B **785**, 441 (2018).

[43] K. Schmidt, R. Borcea, K. Burkard, J. Döring, M. Górska, H. Grawe, W. Hüller, Z. Janas, R. Kirchner, M. L. Commara, C. Mazzocchi, and E. Roeckl, Nucl. Phys. A **701**, 272 (2002).

[44] E. Roeckl, Nucl. Phys. A **704**, 200 (2002).

[45] A. Ahmed, A. V. Ramayya, D. L. Sastry, J. H. Hamilton, R. B. Piercey, H. Kawakami, A. P. de Lima, C. F. Maguire, R. L. Robinson, H. J. Kim, J. C. Wells, and A. C. Rester, Phys. Rev. C **24**, 1486 (1981).

[46] E. McCutchan, Nucl. Data Sheets **113**, 1735 (2012).

[47] T. Kibédi, T. W. Burrows, M. B. Trzhaskovskaya, P. M. Davidson, and C. W. N. Jr., Nucl. Instrum. Methods Phys. Res. Sect. A **589**, 202 (2008).
[48] A. Petrovici, Symmetry **14**, 2594 (2022).
[49] N. Marchini, A. Nannini, M. Rocchini, T. R. Rodríguez, M. Ottanelli, N. Gelli, A. Perego, G. Benzoni, N. Blasi, G. Bocchi, D. Brugnara, A. Buccola, G. Carozzi, A. Goasduff, E. T. Gregor, P. R. John, M. Komorowska, D. Mengoni, F. Recchia, S. Riccetto *et al.*, Phys. Lett. B **844**, 138067 (2023).
[50] A. Davydov and G. Filippov, Nucl. Phys. **8**, 237 (1958).
[51] J. L. Wood, A.-M. Oros-Peusquens, R. Zaballa, J. M. Allmond, and W. D. Kulp, Phys. Rev. C **70**, 024308 (2004).
[52] J. M. Allmond, J. L. Wood, and W. D. Kulp, Phys. Rev. C **81**, 051305(R) (2010).
[53] L. Próchniak and S. G. Rohoziński, J. Phys. G: Nucl. Part. Phys. **36**, 123101 (2009).
[54] L. Próchniak, Phys. Scr. **90**, 114005 (2015).
[55] D. Muir, Microscopic modelling of collective quadrupole excitations of nuclei, Ph.D. thesis, University of York, 2021.
[56] J. Dobaczewski, W. Satuła, B. Carlsson, J. Engel, P. Olbratowski, P. Powałowski, M. Sadziak, J. Sarich, N. Schunck, A. Staszczak, M. Stoitsov, M. Zalewski, and H. Zduńczuk, Comput. Phys. Commun. **180**, 2361 (2009).
[57] M. Kortelainen, T. Lesinski, J. Moré, W. Nazarewicz, J. Sarich, N. Schunck, M. V. Stoitsov, and S. Wild, Phys. Rev. C **82**, 024313 (2010).
[58] M. Kortelainen, J. McDonnell, W. Nazarewicz, P.-G. Reinhard, J. Sarich, N. Schunck, M. V. Stoitsov, and S. M. Wild, Phys. Rev. C **85**, 024304 (2012).
[59] Y. Shi, J. Dobaczewski, and P. T. Greenlees, Phys. Rev. C **89**, 034309 (2014).